Automated stromal nerve rejection in corneal confocal images *in vivo*

Eric N. Brown,[1] Jon J. Camp,[1] Sanjay V. Patel,[2] Jay W. McLaren,[2]
William M. Bourne,[2] Richard A. Robb[1]

Biomedical Imaging Resource[1] and Department of Ophthalmology,[2] Mayo Clinic and Mayo Foundation, Rochester, MN 55905.

ABSTRACT

With the advent of corneal confocal microscopy, investigators can determine keratocyte density in the corneal stroma *in vivo*. We and others have written automated algorithms to measure keratocyte density from human corneal confocal images. Such algorithms are only accurate if they exclude images of stromal nerve bundles (elongated objects) that would otherwise be counted as keratocytes. In this study we devised an algorithm to identify stromal nerve bundles and exclude them from measurements of keratocyte density. Nerve bundles were detected based on their size and aspect ratio, and were then subtracted from images by using a combination of morphology operations and direction calculations. The validity of nerve removal on measurements of keratocyte density was assessed. Keratocyte density was measured from confocal images of three normal human corneas *in vivo* by using our algorithm with nerve removal. After the same eyes underwent enucleation, density was measured manually from histologic sections. Keratocyte density was also measured from confocal images of 57 normal corneas *in vivo* (57 subjects) with and without nerve removal. In the three enucleated eyes, there was no significant difference between keratocyte density measured by automated counting with nerve removal and by histologic methods (P=0.75). However, in the 57 normal corneas, use of the nerve-removal algorithm reduced estimates of density by 57.0 ± 164.6cells/mm^3 (mean ± SD, p<0.038) in the anterior two-thirds of the stroma.

Keywords: Keratocyte, confocal imaging, nerve

1. INTRODUCTION

The introduction of the confocal microscope has opened up the broad research area of ophthalmology research *in vivo*. The ability of this class of microscope to image high resolution, narrow depth-of-field scans of the full-thickness human cornea allows for detailed examination at the cellular level for use in ophthalmology research[1] and in clinics.[2] The corneal stroma accounts for 90% of the thickness of the human cornea,[3] and is lined anteriorly and posteriorly by epithelial and endothelial cells respectively. The corneal stroma predominantly consists of an extracellular matrix of collagen and proteoglycans, and cells called *keratocytes*. Confocal microscopy of the human cornea *in vivo* has been used to study keratocytes and changes in their density after surgery,[2,4,5] contact lens wear,[2] aging,[6] and in pathologic conditions of the cornea.[2] Previously, invasive histologic methods were required to obtain information about the corneal stroma, requiring extensive preparation of enucleated eyes and excised corneas, and such methods are not appropriate for clinical use.[4] With confocal microscopy, the corneal stroma can be examined *in vivo* at the cellular level. Full-thickness confocal microscopy scans of the cornea consist of multiple frames, where each frame in a scan represents a single image of the cornea at a specific z-depth (Figure 1). Thus, a single scan allows for the comparison of corneal characteristics including keratocyte density throughout the full-thickness corneal stroma.

Figure 1. Confocal image of the human cornea *in vivo* containing keratocyte nuclei and a stromal nerve.

Researchers were initially limited to manual inspection of confocal microscopy images,[2,4] which contained large amounts of noise and were of poor contrast. Observers had to painstakingly count the number of keratocyte nuclei, which were represented by bright objects against a dark background (Figure 1), in each image to estimate keratocyte density. Poor contrast and high noise limited the success of early attempts to automate keratocyte density calculations.[7] More recently, we have developed an automated algorithm to analyze confocal microscopy images in

order to measure keratocyte density.[6,8] Our algorithm accounts for noise and the inhomogeneity in contrast and brightness present in confocal images in order to calculate accurate keratocyte densities.

To determine keratocyte density accurately in the stroma of normal human corneas, computer algorithms must be able to distinguish keratocyte nuclei from noise and from stromal nerves, both of which also appear as bright objects. Stromal nerves enter the cornea at the limbus, deep in the mid-stroma, and pass anteriorly toward the corneal epithelium as they pass centrally. Keratocyte nuclei typically appear as small circular or oval objects within the field of view, whereas nerve bundles are characterized by their large, oblong shape and usually span the entire field of view. Objects representing noise are smaller than keratocyte nuclei and can be eliminated based on size alone. If objects representing nerves were not accurately removed from confocal images in the corneal stroma, they would be counted as one or more keratocyte nuclei, and would falsely increase keratocyte density. Furthermore, because each image represents an optical section of stroma approximately 10μm in z-depth, one nerve (or keratocyte nucleus) is visualized in multiple consecutive images. However, the removal of a stromal nerve from an image representing a section of corneal stroma is made difficult by the fact that many objects representing keratocyte nuclei adjoin the object representing a nerve. Simple algorithms designed to subtract the image of the nerve also subtract the adjoining images of keratocyte nuclei. In this paper, we describe a method that removes images of stromal nerves while preserving images of adjoining keratocyte nuclei so that keratocyte density can be accurately measured by an automated algorithm. We then determined the effect of our nerve subtraction method on keratocyte density.

2. METHODS

2.1 Nerve Removal

The automated keratocyte counting algorithm[6,8] developed by the Biomedical Imaging Resource, Mayo Clinic, Rochester, MN, by using the AnalyzeAVW software package[9,10] incorporated a number of filtering,[11] histogram expansion,[11] and morphology operations[12] to produce a binary, segmented image of objects from a single frame in a confocal scan of the human cornea (Figure 2). The binary image contained all objects present in the original confocal image. The goal of nerve detection and removal was to produce a binary, segmented image containing only objects that represented keratocyte nuclei (Figure 3).

After a binary image, which contained objects representing nerves and keratocyte nuclei, was produced, the nerve detection phase was started. Any object that had a larger area than a set threshold (3000 pixels) was a candidate for nerve removal. Because this often included objects that represented clusters of multiple keratocytes, we also needed to determine the aspect ratio of the object, defined as the length of the minor axis of the best fit bounding box divided by the length of the major axis of the best fit bounding box of the object. The smaller the aspect ratio the more elongated the object, which was typical of stromal nerves thus enabling their identification. Nerves were classified as having an aspect ratio of less than 0.45.

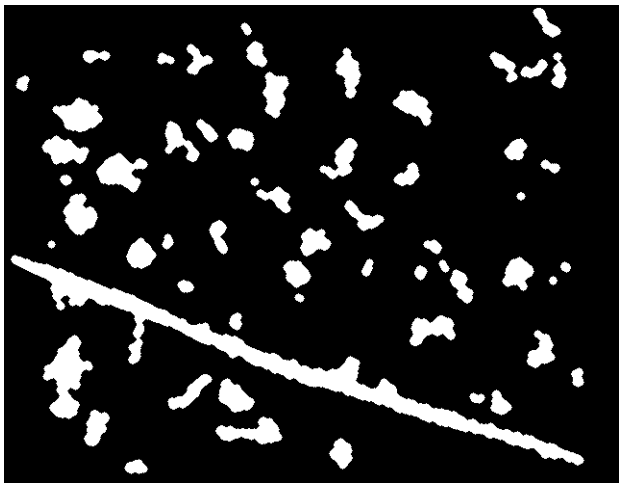

Figure 2. Binary image produced by the Mayo Clinic's autmoated keratocyte counter.

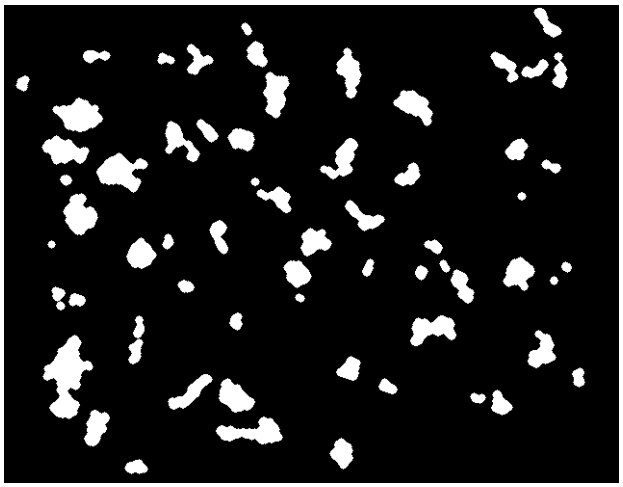

Figure 3. Final binary, segmented confocal image containing keratocyte nuclei including those previously adjoining a nerve.

Figure 4. Multiple fragments of a single nerve with adjoining keratocyte nuclei.

Figure 5. Maximum length internal chord for a nerve fragment with adjoining keratocyte nuclei.

Figure 6. Multiple nerve fragments joined together.

Figure 7. Nerve isolated from a binary object representing a nerve and adjoining keratocyte nuclei.

Figure 8. Keratocyte nuclei adjoining a nerve that were isolated to be included in density measurements.

Unfortunately, the processing steps employed to convert the grayscale confocal image into a binary image often split a single object representing a nerve into multiple fragments (Figure 4). After one fragment of the nerve was detected, all neighboring fragments were joined together. We achieved this by determining the direction of the nerve and joining objects encountered within a fixed distance (15 pixels) of the ends of the nerve to the original nerve. In order to maximize the performance of this phase, the angle of the maximum-length internal chord (Figure 5) of the binary object was used as the direction of the nerve instead of simply using the angle of the best-fit bounding box. This was used because the adjoining objects representing keratocyte nuclei skewed the angle of the best-fit bounding box but did not affect the direction of the maximum-length internal chord. The ends of the internal chord were used as the ends of the nerve in detection of additional nerve fragments. We used the angle of the nerve in conjunction with a morphology close operation to join the fragments together. The elongation phase was repeated until no further fragments could be joined (Figure 6).

When an entire nerve had been detected, it alone was removed while preserving all adjoining keratocyte nuclei. The nerve was first isolated by using a morphology open operation with a stencil composed of a line 50 pixels in length and 1 pixel wide, oriented in the direction of the entire nerve (as computed from the maximum-length internal chord of the object) (Figure 7). The resulting nerve was subtracted from the original binary object and filtered with a small morphology open operation to obtain adjoining keratocyte nuclei (Figure 8). The adjoining keratocyte nuclei were therefore preserved for counting along with other keratocyte nuclei in the frame.

After nerve removal, the resulting objects representing keratocyte nuclei were counted as described in a previous study.[8] Finally, volumetric keratocyte density was obtained using stereologic methods.[13]

2.2 Subjects

Fifty-seven confocal microscopy scans of the central human cornea of 57 subjects were obtained at Mayo Clinic, Rochester, MN. All subjects had normal corneas, had never worn contact lenses, did not use medications that affected the cornea, and had no history of corneal disease or surgery. Subjects were aged from 12 to 80 years and were of either sex and any race.

A Tandem Scanning Confocal Microscope (Tandem Scanning Corporation, Reston, VA), calibrated as outlined in a previous study,[8] was used to obtain corneal scans *in vivo*. The confocal microscope had a 24X, 0.6 NA objective lens with a concave surface and a working distance of 0-1.5 mm. The focal plane of the microscope could be adjusted to varying depths while the position of the front surface of the objective tip remained fixed. The focal plane and image acquisition was controlled from a computer joystick, mounted onto the mechanical joystick of the microscope, and connected to a Silicon Graphics INDY (Silicon Graphics Inc., Mountain View, CA) via an encoder mike controller (Oriel 18011, Oriel Instruments, Stratford, CT). Images 640 by 496 pixels (475µm by 350µm) were obtained from a low-light camera (DAGE_MTI VE-1000 SIT, DAGE_MTI Inc., Michigan City, IN) and were stored on the workstation's hard drive at 30 frames per second.

Proparacaine hydrochloride 0.5% (Bausch & Lomb Pharmaceuticals, Inc., Tampa, FL) was instilled on the eye before examination. The objective lens of the confocal microscope was disinfected with 75% isopropyl alcohol wipes before and after each examination. A drop of 2.5% hydroxypropyl methylcellulose (CIBAVision Ophthalmics, Atlanta, GA) optical coupling medium was placed on the objective lens. The lens was manually advanced until it made contact with the eye. A series of confocal images was acquired (one scan) and digitized directly into the workstation as the focal plane advanced at an average speed of 78μm/sec, or 2.6μm per frame. Three to four scans were acquired from the central cornea of each subject. The best scan, defined as containing little ocular motion and no anteroposterior movement of the cornea relative to the objective, was used for analysis for each subject.

2.3 Analysis

Three corneas of three subjects were scanned with the confocal microscope prior to enucleation of the eyes for choroidal melanomas. Keratocyte density was manually estimated in five equal-thickness sections of the corneal stroma from stained histologic sections. Tissue preparation, cell counting, correction for cell shrinkage, and stereologic methods were used to estimate keratocyte density.[8] Keratocyte density in five equal-thickness regions of the corneal stroma was also estimated by using the automated counter with nerve rejection. These two methods of determining density were compared by using paired Student's *t*-tests to confirm that the automated algorithm with nerve rejection was valid for measuring keratocyte density in normal human corneas *in vivo*.

Forty confocal images with 17 containing nerves were randomly acquired from 20 scans. Two masked human observers manually identified nerves and adjoining keratocytes in each of these images. The results of manual identification were compared to the results obtained by the automated nerve detection and removal algorithm to assess the sensitivity of the algorithm.

Keratocyte density with and without nerve removal was computed for the 57 normal human scans by using the keratocyte counter algorithm. Mean keratocyte density was computed in five anteroposterior regions of the corneal stroma: the anterior 10% of stroma, the remainder of the anterior one-third of stroma, the central one-third of stroma, the posterior 10% of stroma, and the remainder of the posterior one-third of the stroma. Two-tailed paired Student's *t*-tests were used to compare keratocyte density of the full-thickness stroma and each anteroposterior stromal region measured with and without the nerve removal algorithm. Descriptive statistics showed the effect of nerve removal on individual frames with and without the presence of nerves.

3. RESULTS

There was no significant difference between keratocyte density calculated by the automated algorithm with nerve removal and keratocyte density manually determined from histologic sections (P=0.75).

The automated nerve detection algorithm correctly detected twelve of the 17 confocal images containing nerves. Of the images that contained nerves, only one adjoining keratocyte out of 15 was not correctly included in the final binary image. There were, however, eleven false positive identifications of adjoining keratocytes.

Nerve rejection had a significant impact on keratocyte density estimation for the anterior two-thirds of the stroma (Table 1). There was no significant difference between keratocyte density in the posterior third of the stroma measured with and

Table 1. Keratocyte density computed with and without nerve rejection by anteroposterior stromal region.

Stromal Depth	Keratocyte Density (cells/mm^3, Mean ± SD, n=57)		P*
(% stromal thickness)	Without Nerve Rejection	With Nerve Rejection	(n=57)
Full-thickness stroma	23959.9 ± 4225.2	23892.1 ± 4245.1	<0.001
0-10% (anterior)	29307.6 ± 4934.6	29231.1 ± 4944.8	0.038
11-33%	24378.8 ± 3269.0	24243.4 ± 3279.0	<0.001
34-66%	22535.0 ± 2906.5	22493.8 ± 2914.9	0.017
67-90%	22243.0 ± 2509.1	22223.8 ± 2530.0	0.257
91-100% (posterior)	22815.0 ± 2671.8	22818.8 ± 2682.0	0.866

* Two-tailed paired Student's *t*-tests, n=57

without nerve rejection ($p>0.05$). Full-thickness keratocyte density decreased by 57.0 ± 164.6cells/mm^3 (mean ± SD) as a result of nerve rejection ($p<0.001$). In frames that contained nerves, keratocyte density decreased by 757.1 ± 1453.9cells/mm^3 when measured with the nerve removal algorithm compared to without the algorithm. Of the 546 frames that contained images of nerves, keratocyte density calculated with nerve removal decreased in 73% of the frames resulting in an average decrease of 1287.6 ± 1188.2cells/mm^3 (n=410) and increased in 23% of the frames (810.6 ± 1079.1cells/mm^3, n=131). Keratocyte density increased by 5.7 ± 595.9cells/mm^3 (n=4471) in the frames that did not contain nerves.

4. DISCUSSION

We have demonstrated that keratocyte density measurement with stromal nerve removal by the computer algorithm was valid by comparing to gold-standard measurements of keratocyte density determined manually from histologic sections. We have devised a method of distinguishing stromal nerves from keratocyte nuclei in confocal microscopy images *in vivo* so that accurate measurements of keratocyte density can be made.

Nerve detection sensitivity was 70% with the automated method presented in this study. Errors in the simple detection scheme were due to difficulties in classifying small, greatly fragmented, or branched nerves. Currently, we are considering Bayesian approaches to improve the accuracy of object segmentation and classification. The high number of false positive adjoining keratocytes may also be improved with such methods.

Nerve removal only had a significant effect on keratocyte density in the anterior two-thirds of the stroma and in the full-thickness stroma (Table 1). No significant difference was found when measuring keratocyte density in the posterior one-third of the stroma with or without the nerve rejection algorithm. The latter can be explained by the fact that stromal nerves enter the cornea at the limbus at mid-stromal depth before passing anteriorly; stromal nerves are not found in the posterior stroma.

Although statistical analysis showed a significant difference between keratocyte densities obtained with and without nerve rejection in the anterior two-thirds of the stroma, a definitive effect on density was not apparent. Overall, a net decrease in keratocyte density was seen with the inclusion of nerve rejection. The alteration on keratocyte density was due to two competing effects of nerve removal: a definite decrease in density for the frame that contained the nerve and the possibility of an increase in density for subsequent frames in a scan.

The direct effect of removing a nerve from a confocal image was the decrease in the number of objects counted. Instead of the nerve and adjoining keratocyte nuclei all being counted as multiple keratocytes, only the adjoining keratocyte nuclei were counted. The decrease in the density of a single frame was 757.1cells/mm^3 for all images containing nerves in the 57 scans examined. Of the images with nerves, the vast majority showed a decrease in keratocyte density.

For frames subsequent to frames containing nerves, keratocyte density may have increased slightly due to progressive adjustments made by the algorithm when determining which objects represented single keratocyte nuclei. At the beginning of each scan, the maximum size for a single keratocyte nucleus was 625 pixels (maximum-size threshold for a single keratocyte nuclei). Objects larger than 625 pixels were assumed to be clusters of multiple keratocyte nuclei and were counted accordingly. After the first image was processed, the maximum-size threshold for the subsequent image was adjusted to reflect the mean size of single keratocytes in the first frame; this enabled the algorithm to adapt to changes in keratocyte size with increasing *z*-depth in the stoma.[8] The number of keratocytes counted per large cluster of nuclei was partly dependent on the mean size of single keratocyte nuclei in the previous frame.[8] If a nerve had many adjoining keratocyte nuclei, these were included in the adjustment the maximum-size threshold when nerve removal was present; however, when nerve removal was not activated they would have been considered part of a large cluster of nuclei and therefore not have had any effect on the maximum-size threshold. The objects representing adjoining keratocyte nuclei that remained after subtraction of nerves were often smaller than objects representing single keratocyte nuclei that did not adjoin nerves. This had the effect of decreasing the mean size of single keratocytes in an individual frame, causing a decrease in the maximum-size threshold, and resulting in more objects being counted as multiple keratocytes. In addition, the decrease in the mean size of keratocytes led to a single multiple-keratocyte object being over-counted. The net effect was a possible increase in the apparent number of keratocytes in subsequent frames of the scan, the presence and magnitude of which depended on the number and size of adjoining keratocyte nuclei to the nerve. Because recent frames had a greater effect on the current maximum-size threshold, the effects of a single nerve were diminished in the long term thus making the increase in density temporary. Therefore, nerves present in the anterior of the stroma had minimal effect on keratocyte density in the posterior of the stroma resulting in no significant difference between keratocyte densities in this region as calculated with and without nerve removal (Table 1).

The effects of nerve removal on keratocyte density across a large *z*-depth of stroma containing nerves, or the stroma as a whole, were significant but not dramatic. This was partly due to the limited number of nerves encountered in the central cornea. Nerve removal would have a greater impact on keratocyte density when a smaller z-depth thickness of the cornea is examined. In situations such as post-operative analysis, keratocyte density may be measured across small z-depths in proximity to the surgical area. In such thin sections of the stroma, a single nerve would have a large effect on calculated keratocyte density if not subtracted from images. Even across large *z*-depths of the cornea, the inclusion of nerve removal ensures that our algorithm is as accurate as possible instead of merely ignoring stromal nerves.

ACKNOWLEDGEMENTS

The authors thank E. Brian Welch, Elson Liu, and David Holmes III (Biomedical Imaging Resource, Mayo Clinic and Mayo Foundation, Rochester, MN) for their help with the design of the nerve rejection algorithm.

REFERENCES

1. W. M. Petroll, J. V. Jester, H. D. Cavanagh, "In vivo confocal imaging," *International Review of Experimental Pathology*, **36**, pp. 93-129, 1996.
2. H. D. Cavanagh, W. M. Petroll, H. Alizadeh, Y. G. He, J. P. McCulley, J. V. Jester, "Clinical and diagnostic use of in vivo confocal microscopy in patients with corneal disease," *Ophthalmology*, **100**, pp. 1444-1454, 1993.
3. H. F. Li, W. M. Petroll, T. Møller-Pedersen, J. K. Maurer, H. D. Cavanagh, J. V. Jester, "Epithelial and corneal thickness measurements by *in vivo* confocal microscopy through focusing (CMTF)," *Curr Eye Res*, **16**, pp. 214-221, 1997.
4. T. Møller-Pedersen, H. F. Li, W. M. Petroll, H. D. Cavanagh, J. V. Jester, "Confocal microscopic characterization of wound repair after photorefractive keratectomy," *Invest Ophthalmol Vis Sci*, **39**, pp. 487-501, 1998.
5. T. Møller-Pedersen, M. Vogel, H. F. Li, W. M. Petroll, H. D. Cavanagh, J. V. Jester, "Quantification of stromal thinning, epithelial thickness, and corneal haze after photorefractive keratectomy using in vivo confocal microscopy," *Ophthalmology*, **104**, pp. 360-368, 1997.
6. S. V. Patel, J. W. McLaren, J. J. Camp, E. N Brown, D. O Hodge, W. M. Bourne, "Normal human keratocyte density and corneal thickness measurement by using confocal microscopy *in vivo*," *Submitted to Investigative Ophthalmology and Visual Science*.
7. J. I. Prydal, F. Franc, P. N. Dilly, M. G. Kerr Muir, M. C. Corbett, J. Marshall, "Keratocyte density and size in conscious humans by digital image analysis of confocal images," *Eye*, **12**, pp. 337-342, 1998.
8. S. V. Patel, J. W. McLaren, J. J. Camp, L. R. Nelson, W. M. Bourne, "Automated quantification of keratocyte density by using confocal microscopy in vivo," *Invest Ophthalmol Vis Sci*, **40**, pp. 320-326, 1999.
9. D. P. Hanson, R. A. Robb, S. Aharon, et al, "New software toolkits for comprehensive visualization and analysis of three-dimensional multimodal biomedical images," *J Digit Imaging*, **10**, pp. 229-230, 1997.
10. R. A. Robb, D. P. Hanson, "ANALYZE: a software system for biomedical image analysis," *Proceedings of First Conference on Visualization in Biomedical Computing, Atlanta, GA, May 22-25*, pp. 507-518, 1990.
11. A. K. Jain, *Fundamentals of Digital Image Processing*, Prentice Hall, Englewood Cliffs, NJ, 1990.
12. K. H. Hohne, W. A. Hanson, "Interactive 3D segmentation of MRI and CT volumes using morphological operations," *J Comput Assist Tomogr*, **16**, pp. 285-294, 1992.
13. E. R. Weibel, *Stereological methods. Practical methods for assessing agreement between two methods of clinical measurement*, Vol 1, Academic Press, London, 1979.